Results of metallographical post-test examinations by RIAR

A. V. Goryachev, I. A. Ivanova
FSUE “SCC-RIAR”, Dimitrovgrad

Introduction

After the test the bundle was filled with epoxy resin and cut into samples in order to examine oxidation of the claddings. Five samples were delivered for examinations to RIAR and five samples were investigated in FZK. The RIAR and FZK samples are similar and represent the planes formed as a result of the bundle cutting (the bottom planes were investigated at FZK, and the top ones - at RIAR).

The task of the samples examination was to estimate oxidation of the claddings, to reveal possible heterogeneity of the temperature in the investigated bundle sections, on the basis of the obtained results to assess reliability of the on-line thermocouple readings and the results of the measurement of integrated hydrogen release.

Oxidation of the claddings is estimated by the results of measurement of thickness of unoxidized claddings layer and the thickness of the formed zirconia and alpha zirconium layers, stabilized by oxygen, using a metallographic microscope.

The objective of this work is presentation of the results obtained on the samples investigated in RIAR and their comparison with the results obtained on similar FZK samples as well as revealing possible systematic discrepancies related to identification of the boundaries of the measured layers and differences in methodical approaches to the measurement techniques.

Description of the examined sections

Pictures of the examined samples are demonstrated in Fig. 1.

Section 554 mm

In section 554 mm the bundle is not deformed. The outer surface of the simulator claddings is uniformly oxidized and obviously there is a spalling effect in the oxides formed on the cladding surface. This effect is typical of alloy E110 at temperatures of 950 - 1050 °C (temperatures during the test are measured by TC located on the claddings). In the space between the simulators the fragments of oxide films and oxidized claddings from the upper sections are observed.

Measurements of thickness of the layers formed in this section are made in four points of each simulator cladding with an azimuth pitch of 90°. Results of measurements are summarized in Table 1. It is necessary to note, that the cladding surface oxide spalling effect in all the investigated sections essentially reduces reliability of the claddings oxidation estimation by the results of measurements of the thickness of formed ZrO_2 layer. In this case the cladding oxidation can be estimated by the results of measurement of the cladding thickness after the test. The diagrams (Fig. 2) show relative changes of the averaged residual thickness of the cladding metal part and thickness of α-Zr (O) layers.

Fig. 3 demonstrates typical structures of the simulator claddings.

Section 654 mm

In section 654 mm (the cladding temperature measured by TC during preliminary oxidation was 1050-1150 °C) the bundle is deformed. The outer surface of the simulator claddings is uniformly oxidized. In this section there are no fragments of the claddings in the space between the simulators. Results of measurements of the layer thickness in this section are summarized in Table 2. Fig. 4 and 5 show the diagrams of the averaged thickness of the measured layers and typical structures of the claddings.

Section 754 mm

This section has no essential qualitative differences from the section 654 mm described above. The temperature measured by TC on the claddings during preliminary oxidation in section 754 mm made up 1100-1200 °C that resulted in a smaller spalling effect of the formed oxides. Results of measurements of the layer thickness in this section are summarized in Table 3 and in the diagram (Fig. 6). Typical cladding structures are shown in Fig. 7.

Section 854 mm

The given section differs from the sections described above by essentially greater simulator cladding oxidation. The temperature measured by TC located on the claddings during preliminary oxidation was equal to 1250-1350 °C. Melt drops are observed in the gap between the simulators. The maximum temperature measured in this section before quenching made up 1900 °C that is close to the melting temperature of α-Zr (O) phase (1970 °C). However, no melt is observed in this section (metallographic examinations show that all the metal phase in this section consists of αZr(O)). The simulator claddings have through-wall cracks. Part of the claddings completely failed and crumbled. Two simulators without a tungsten rod in the centre of the pellets are destroyed in this section. It is necessary to note, that the surfaces of the cracks in the simulator claddings are not oxidized,

that testifies to the fact that their damage occurred at the reflood stage. Absence of the cracks surface oxidation also points at the fact that the process of their damage does not make essential contribution to hydrogen production at the reflood stage. Results of examinations of this section are summarized in Table 4 and Fig. 8 and 9.

Section 954 mm

In this section we observed melting and full oxidation of the simulator claddings (Fig. 10). The measured claddings temperature during preliminary oxidation made up 1300 – 1450 °C. The maximum temperature before quenching was about 2000 °C. The bundle shroud also melted.

Due to through oxidation of the claddings in this section, their essential deformation and complete loss on a number of simulators, quantitative measurements were not done. The structure of the formed melt is shown in Fig.11.

By the results of examination of five sections it is possible to conclude that the most reasonable parameter to assess the claddings oxidation level is the results of measurement of the residual metal layer thickness. In the lower sections (554 and 654 mm) we observe non-uniformity of oxidation, which is apparently caused by a radial thermal gradient in the direction of 180°. In section 754 mm the claddings oxidation is more uniform across the section, thermal gradient may also be observed in the direction of 180°. Section 854 mm exhibits essential non-uniformity of the claddings oxidation presumably owing to a strong radial thermal gradient in the direction of 315°. Fig.13 demonstrates a diagram of thickness of the residual cladding metal part of all the examined sections. Fig.14 shows a diagram of the α-Zr (O) layers thickness in the investigated sections that exhibits similar periodicity of thickness changes in the sections. However, it is necessary to note smaller reliability of these data because of difficulty in identification of the layer boundaries and thorough transformation of the cladding metal to α-Zr (O) in the top sections.

Measurement of oxidation of the withdrawn rods

Two of the three rods 6 mm in diameter located at the periphery of the bundle were withdrawn at intermediate stages of the test - 60 seconds prior to the termination of the preliminary oxidation stage (rod D) and before quenching at approximately maximum temperature of the bundle (rod F). Rod B was withdrawn from the bundle after the test termination. It is necessary to compare oxidation levels of these rods in order to assess kinetics of the cladding oxidation during the test.

As well as on the simulator claddings, the effect of oxide film spalling is distinctly observed on the withdrawn rods. Therefore the results of ZrO_2 layer thickness measurements cannot be used to assess oxidation. To compare oxidation of the withdrawn

rods, residual metal parts of the rods were measured. The area of the metal part of the rods at the investigated elevations was measured by the pictures of the cross-sections made with 12x magnification using a method of the image quantitative analysis. The diameter of an equidimensional circle was calculated by the results of measurements. Difference in the measured and initial (6 mm) rod diameters was taken as the extent of oxidation.

Photos of the examined sections are shown in Fig. 12. Table 2 contains the results of measurements and calculations.

Conclusions

1. Results of the measurements do not contradict the results of the on-line temperature measurements.
2. The sections revealed essential non-uniformity of the claddings oxidation that allows to assume existence of radial thermal gradients during the test.
3. Observable cracks and sites of the cladding damage are not oxidized, that testifies to the fact that the claddings are damaged at the stage of quenching and that this process has small influence on hydrogen generation at the end of the test.
4. Formation and essential oxidation of the claddings melt shows that it could make considerable contribution to the observed increased generation of hydrogen both during preliminary oxidation and at the stage of quenching.

Table 1. Results of measurement of the average thickness of QUENCH simulator layers in different sections

Rod No.	Layer	Section coordinate, mm			
		554	654	754	854
		Average layer thickness, μm			
1	ZrO_2 (outer)		60	89	
	α-layer (outer)	57	76	126	
	Me	623	617	605	
2	ZrO_2 (outer)		37	81	354
	α-layer (outer)	55	71	115	
	Me	633	637	628	439
3	ZrO_2 (outer)	16	34	74	
	α-layer (outer)	56	57	97	
	Me	638	643	622	
4	ZrO_2 (outer)	17	39	84	
	α-layer (outer)	58	62	110	
	Me	637	631	624	
5	ZrO_2 (outer)	21	46	83	
	α-layer (outer)	61	66	99	
	Me	639	636	623	
6	ZrO_2 (outer)	20	49	74	314
	α-layer (outer)	58	72	108	
	Me	634	634	630	410
7	ZrO_2 (outer)		46	80	337
	α-layer (outer)	54	65	112	
	Me	634	632	629	347
8	ZrO_2(outer)			53	243
	α-layer (outer)	41	58	108	277
	Me	664	631	639	499
9	ZrO_2(outer)		27	54	299
	α-layer (outer)	36	49	89	
	Me	660	633	635	480
10	ZrO_2(outer)		22	47	
	α-layer (outer)	37	43	78	
	Me	662	638	633	

Rod No.	Layer	Section coordinate, mm			
		554	654	754	854
		Average layer thickness, μm			
11	ZrO_2(outer)		25	62	
	α-layer (outer)	40	66	90	
	Me	660	630	629	
12	ZrO_2(outer)		26	61	
	α-layer (outer)	40	65	94	
	Me	667	639	626	
13	ZrO_2(outer)		26	62	
	α-layer (outer)	38	53	96	
	Me	659	660	626	
14	ZrO_2(outer)		25	53	
	α-layer (outer)	36	74	114	
	Me	658	646	632	
15	ZrO_2 (outer)	12	29	47	251
	α-layer (outer)	37	80	110	198
	Me	654	640	636	510
16	ZrO_2 (outer)	11	28	46	167
	α-layer (outer)	32	81	102	165
	Me	653	644	638	574
17	ZrO_2 (outer)		37	51	276
	α-layer (outer)	41	89	112	
	Me	646	633	624	471
18	ZrO_2 (outer)		26	51	306
	α-layer (outer)	41	75	107	
	Me	640	632	636	434
19	ZrO_2 (outer)		30	61	283
	α-layer (outer)	38	76	125	
	Me	652	635	627	492
20	ZrO_2 (outer)	12	27	66	259
	α-layer (outer)	43	77	92	
	Me	655	649	634	452
21	ZrO_2 (outer)		29	62	
	α-layer (outer)	40	65	84	
	Me	648	630	629	

Rod No.	Layer	Section coordinate, mm			
		554	654	754	854
		Average layer thickness, μm			
22	ZrO_2 (outer)		35	71	
	α-layer (outer)	40	68	106	
	Me	653	644	632	
23	ZrO_2 (outer)		30	76	
	α-layer (outer)	52	70	99	
	Me	656	652	631	
24	ZrO_2 (outer)		28	71	
	α-layer (outer)	47	67	97	
	Me	651	644	630	
25	ZrO_2 (outer)		28	69	240
	α-layer (outer)	39	79	126	
	Me	632	644	621	515
26	ZrO_2 (outer)	18	32	65	253
	α-layer (outer)	45	84	133	
	Me	639	642	623	484
27	ZrO_2 (outer)		31	59	197
	α-layer (outer)	43	94	118	
	Me	641	642	633	550
28	ZrO_2 (outer)		32	62	248
	α-layer (outer)	43	84	96	
	Me	647	649	643	505
29	ZrO_2 (outer)		31	65	314
	α-layer (outer)	43	83	95	
	Me	640	637	640	455
30	ZrO_2 (outer)		27	68	284
	α-layer (outer)	41	84	93	
	Me	639	638	629	455
31	ZrO_2 (outer)		28	61	248
	α-layer (outer)	52	80	104	
	Me	624	634	626	489

Table 2. Results of measurement of the withdrawn rod oxidation

Rod designation	Holder designation		Thickness of α-layer, μm	$S_{rod\ section}$, mm^2	$D_{measured}$, mm	$\delta_{oxide\ film}$, μm
D	D1 ~700- 680 mm		39	28.1	5.98	11
			37			
			37			
		Average	**38**			
		RMSD	**1**			
	D3 ~940 - 920 mm		109	26.6	5.82	89
			151			
			163			
			164			
		Average	**147**			
		RMSD	**26**			
	D2 ~1120 - 1100 mm		50	28.2	5.99	4
			52			
		Average	**51**			
		RMSD	**2**			
F	F2 ~700 - 680 mm		74	27.1	5.88	61
			65			
			37			
		Average	**59**			
		RMSD	**19**			
	F1 ~940 - 920 mm		205	24.5	5.58	209
			201			
		Average	**203**			
		RMSD	**3**			
	F3 ~1120-1100 mm		66	26.4	5.80	102
			70			
			68			
		RMSD	**2**			
B	B2 ~700 - 680 mm		31	27.9	5.96	18
			26			
			32			
			35			
		Average	**31**			
		RMSD	**4**			
	B1 ~820 - 800 mm		120	25.9	5.74	130
			126			
			118			
		Average	**121**			
		RMSD	**5**			

Description of the examined sections

Pictures of the examined samples are demonstrated in Fig.3.

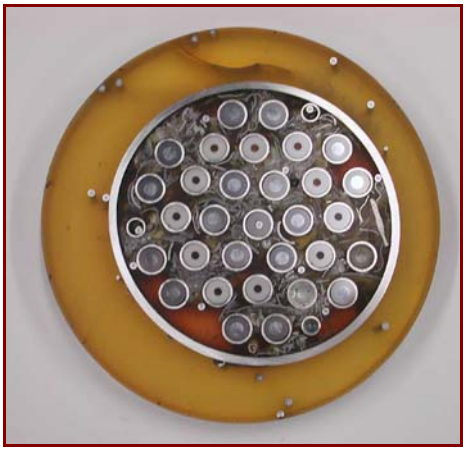

Sample 554 mm, bottom view

Sample 654 mm, bottom view

Sample 754 mm, bottom view

Sample 854 mm, bottom view

Sample 954 mm, bottom view

Fig. 1. Appearance of the examined sections.

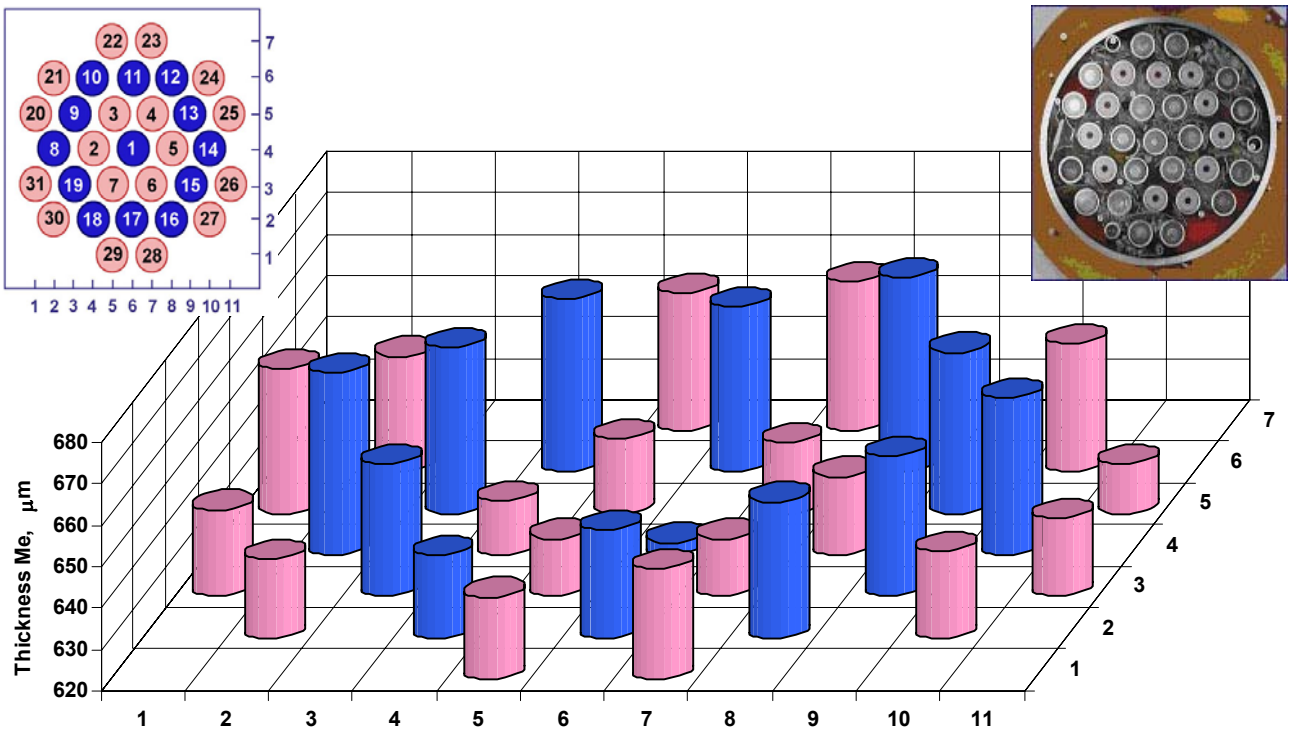

Fig. 2. Diagram of change in the thickness of metal part of the simulator claddings in section 554 mm.

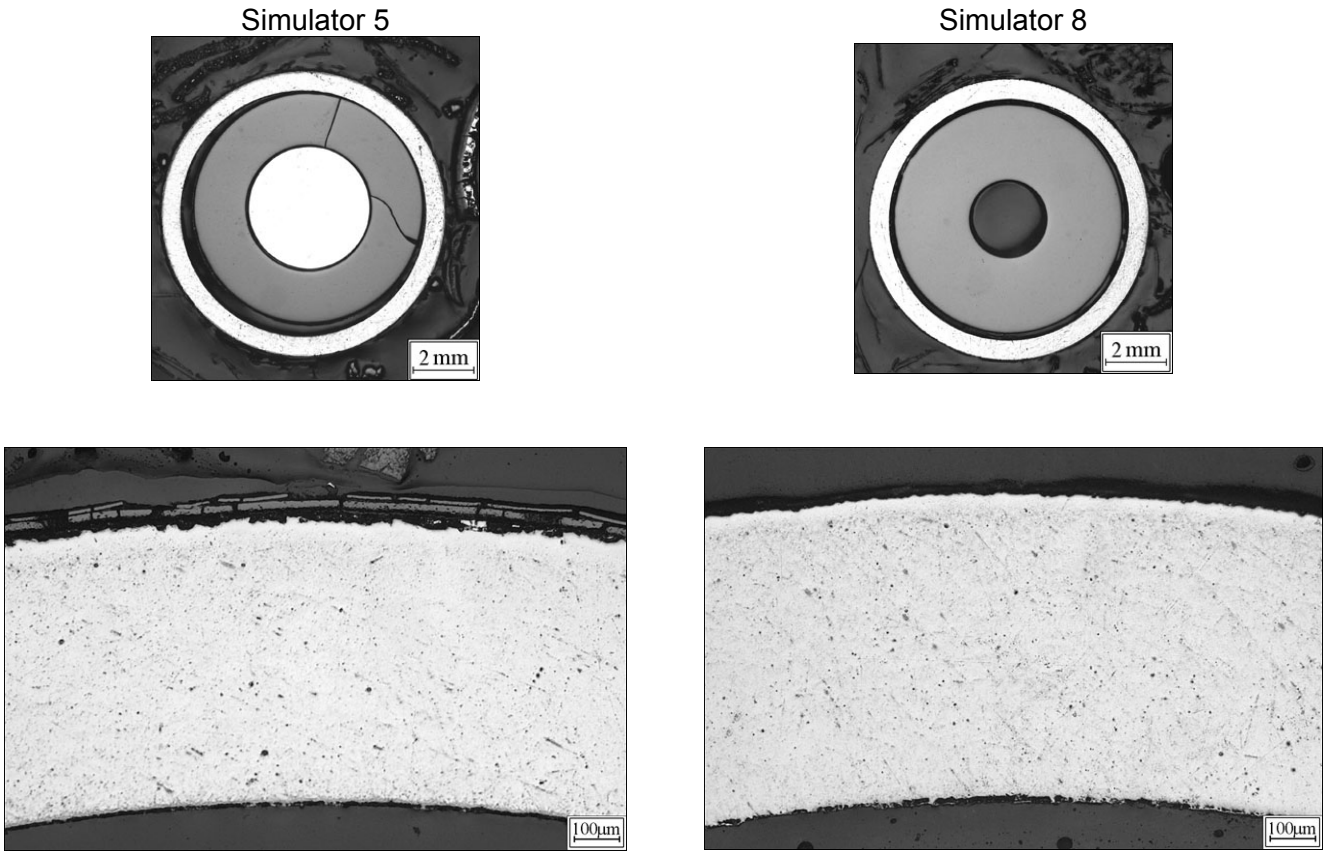

Fig. 3. Structure of the simulator claddings in section 554 mm.

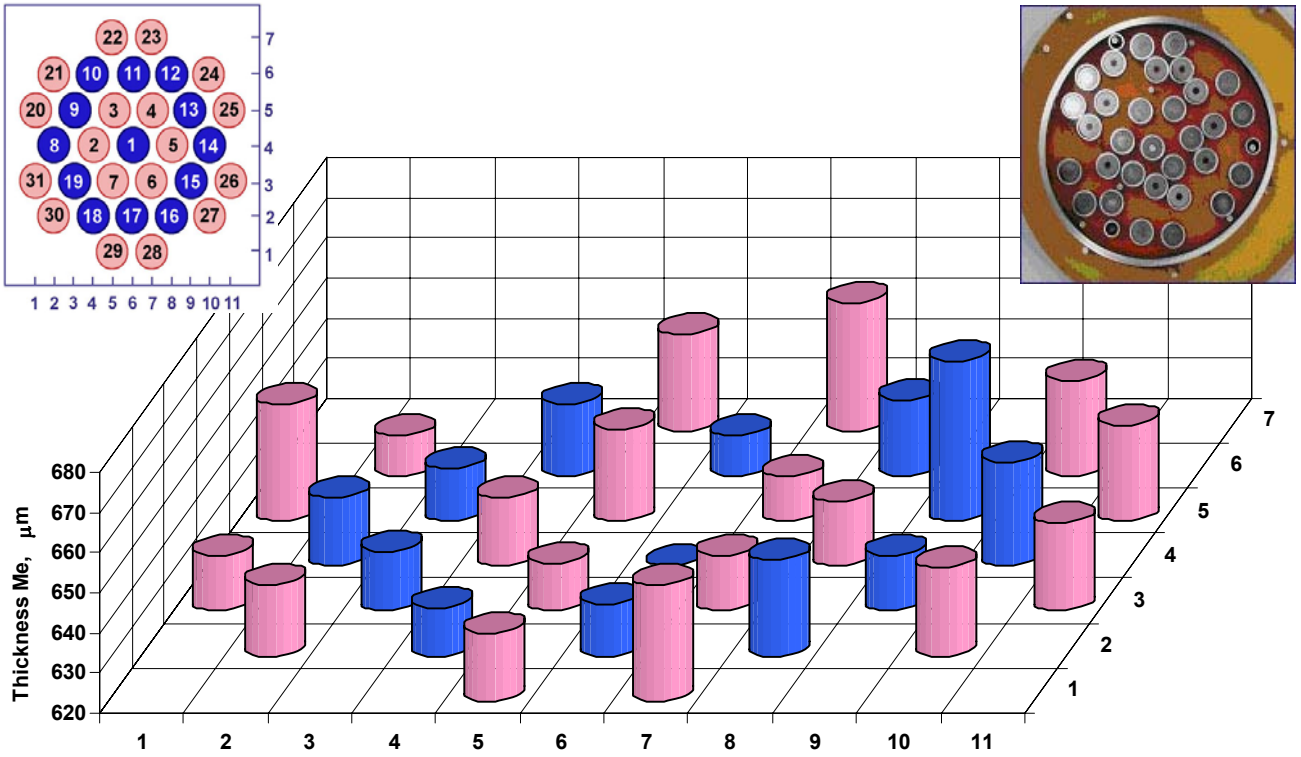

Fig. 4. Diagram of change in the thickness of metal part of the simulator claddings in section 654 mm.

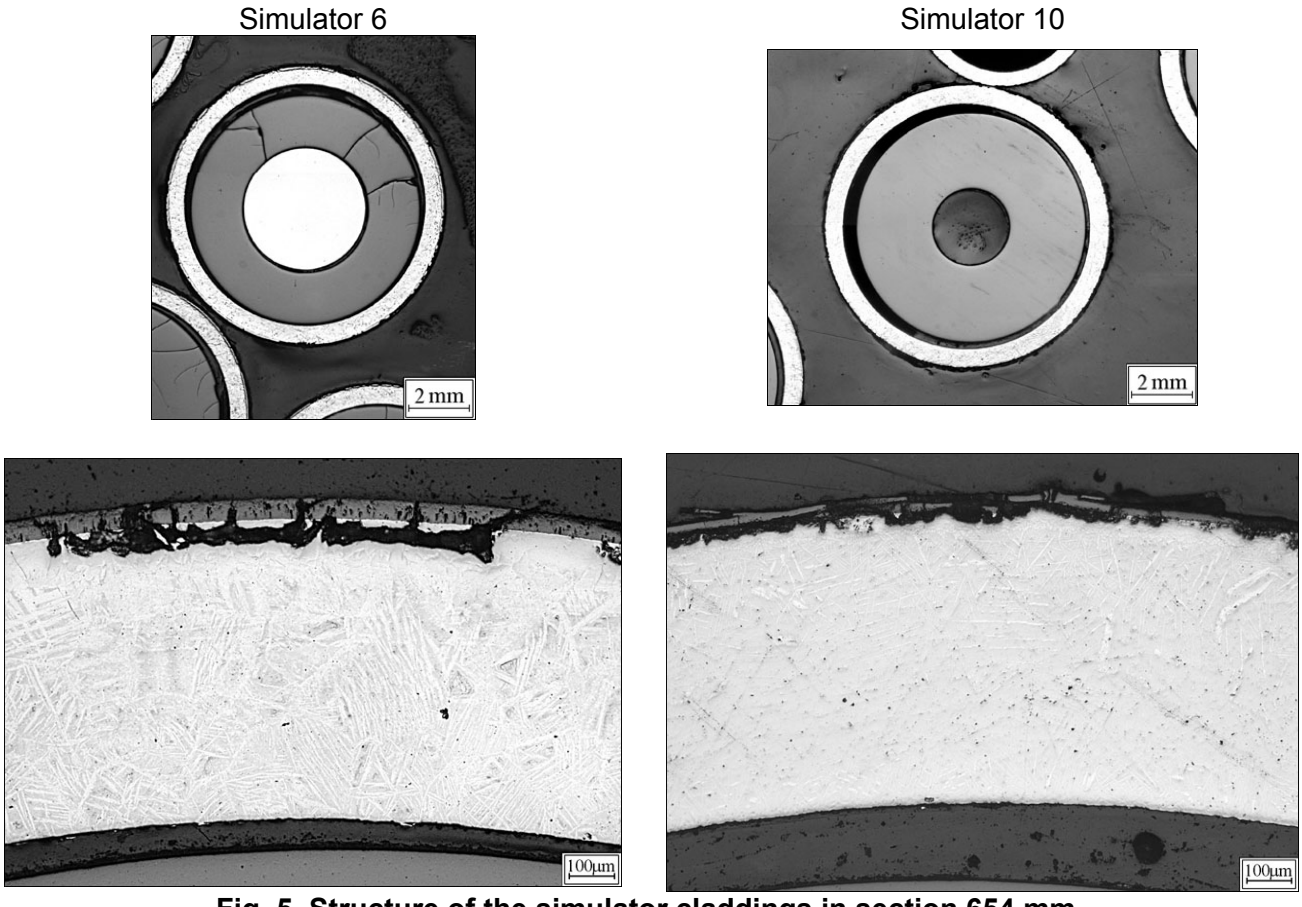

Fig. 5. Structure of the simulator claddings in section 654 mm.

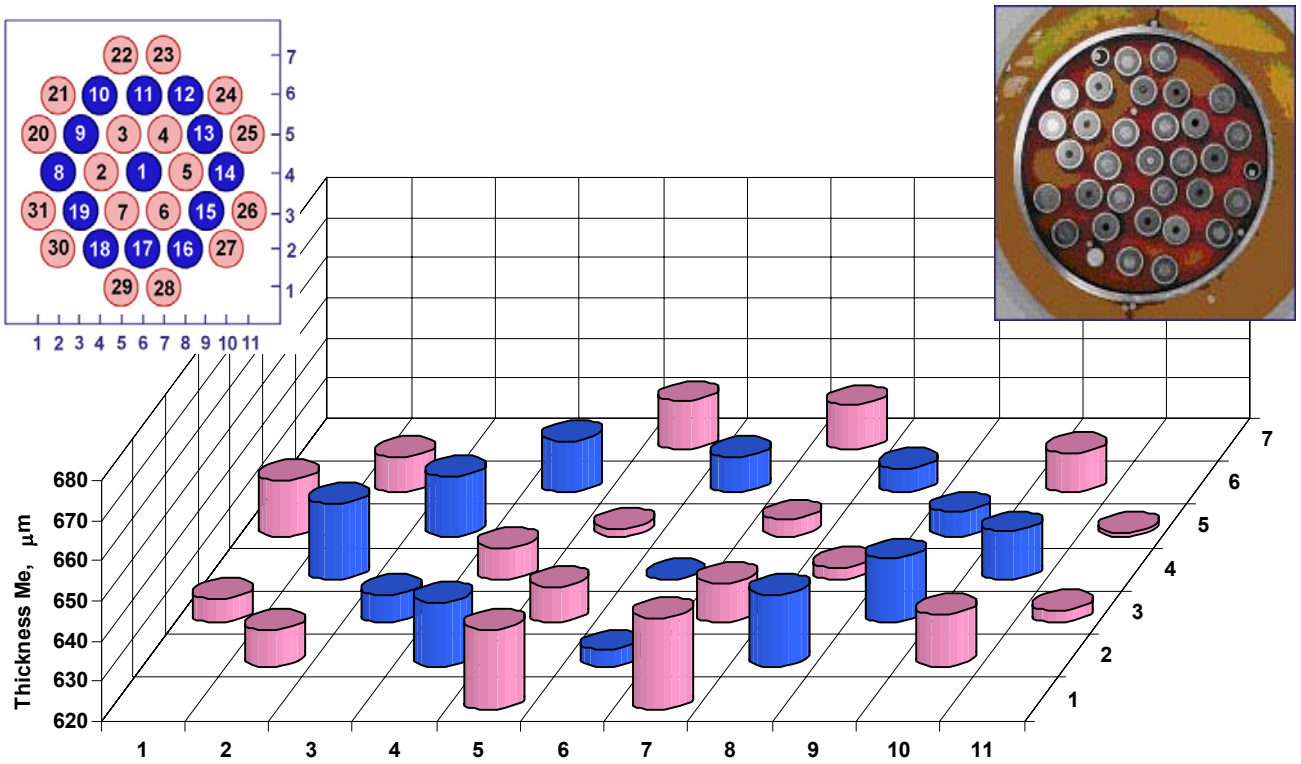

Fig. 6. Diagram of change in the thickness of metal part of the simulator claddings in section 754 mm.

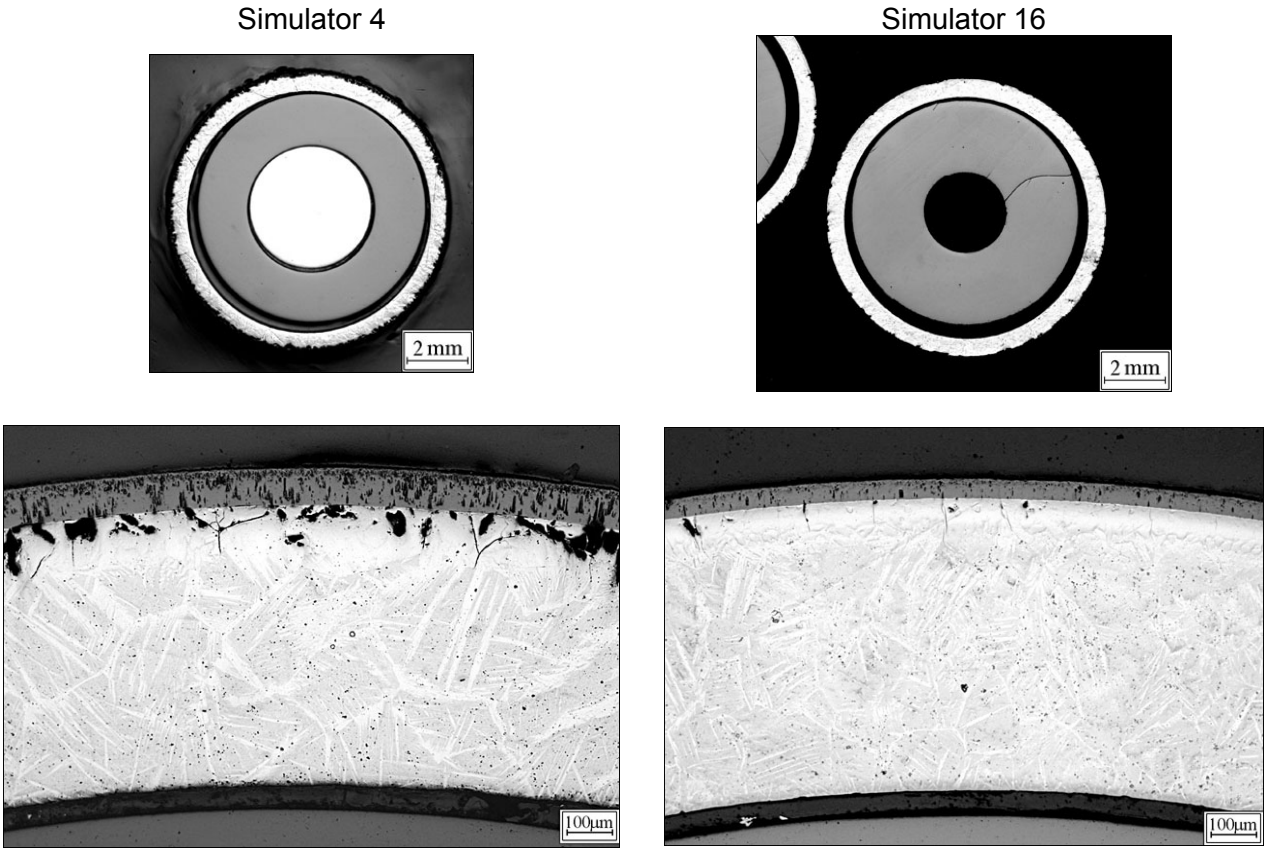

Fig. 7. Structure of the simulator claddings in section 754 mm.

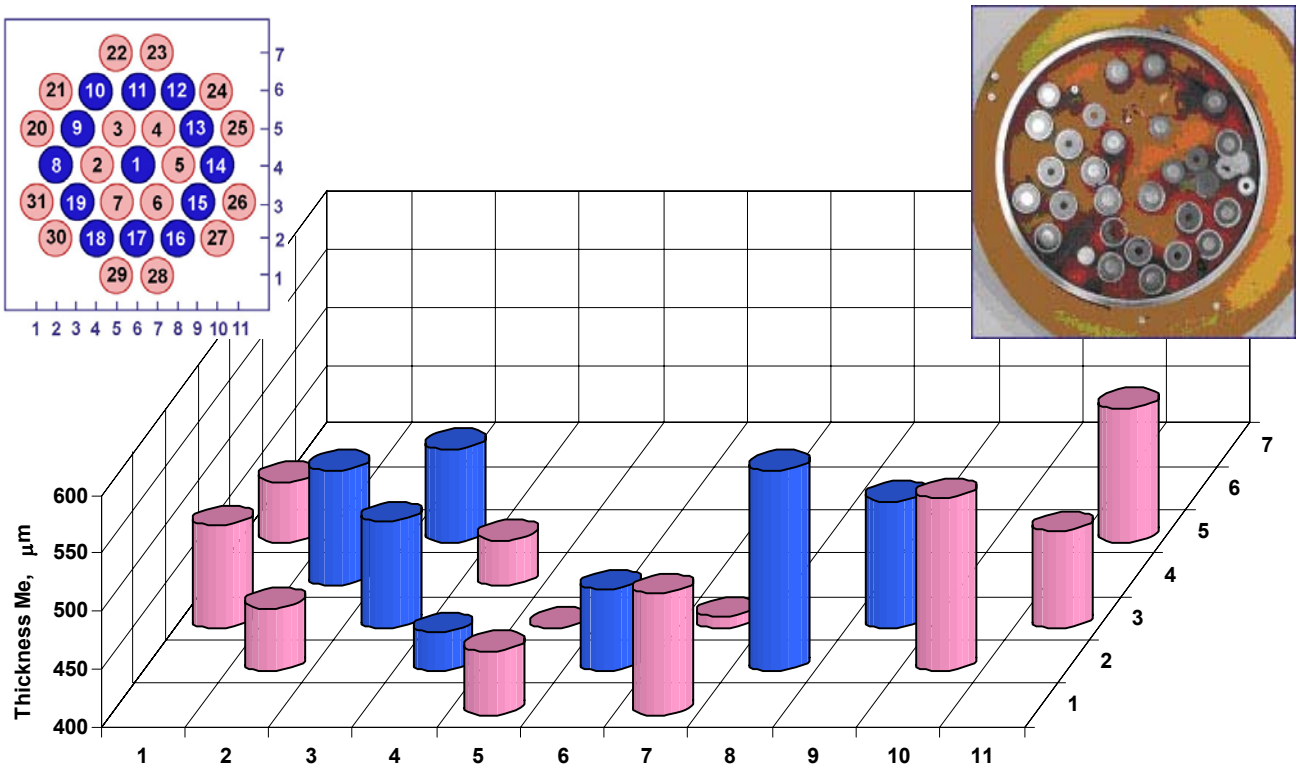

Fig. 8. Diagram of change in the thickness of metal part of the simulator claddings in section 854 mm.

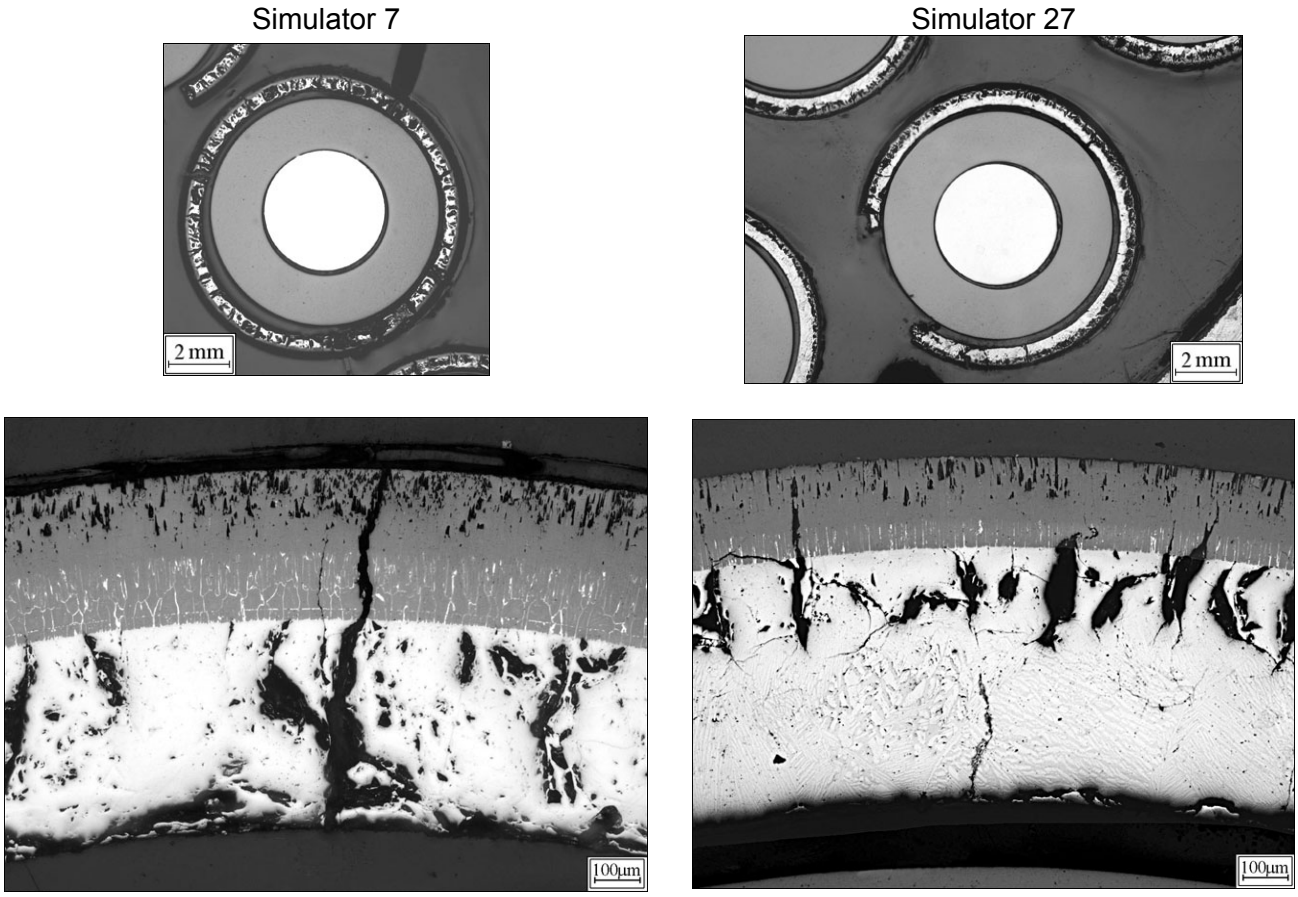

Fig. 9. Structure of the simulator claddings in section 854 mm.

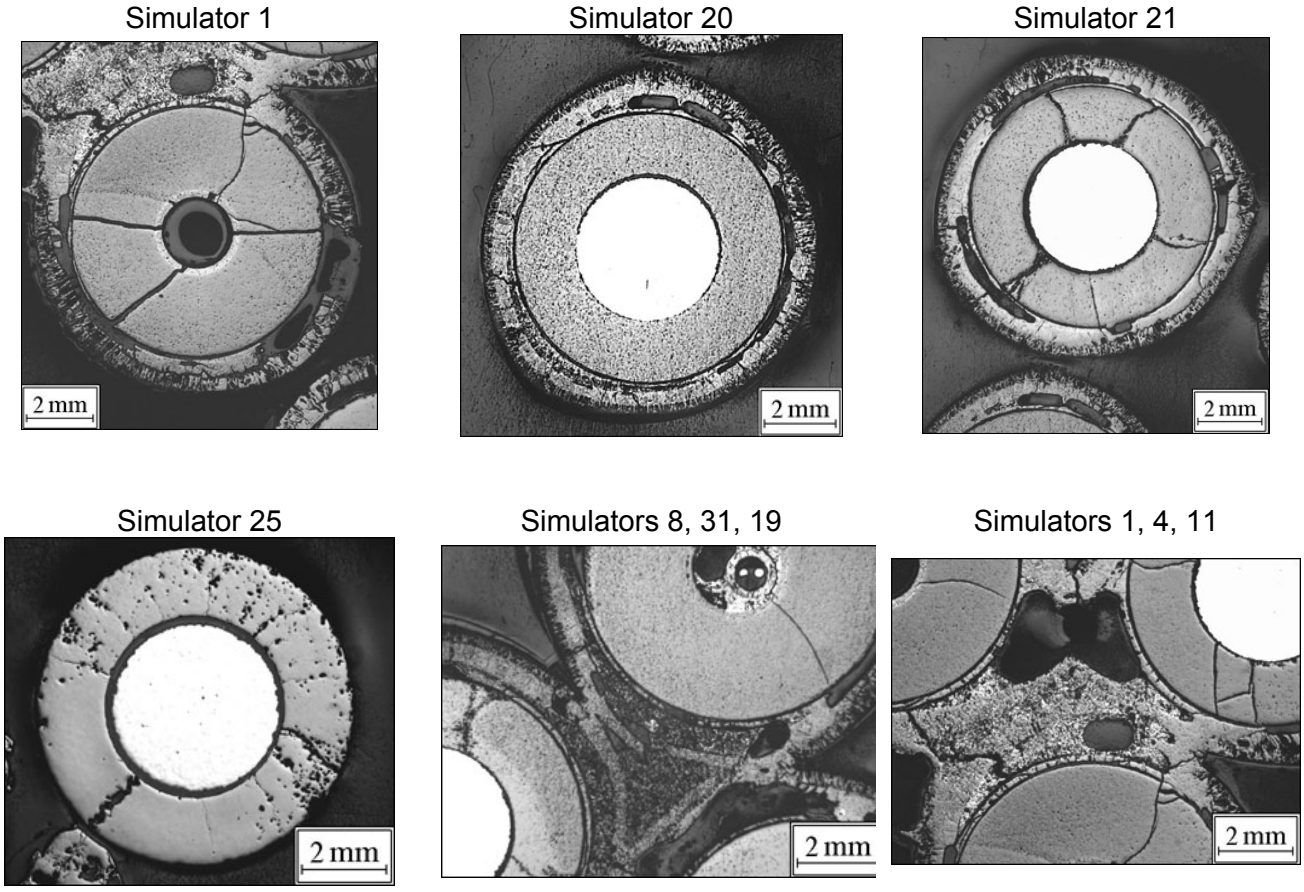

Fig. 10. Macrographs of the simulators in section 954 mm.

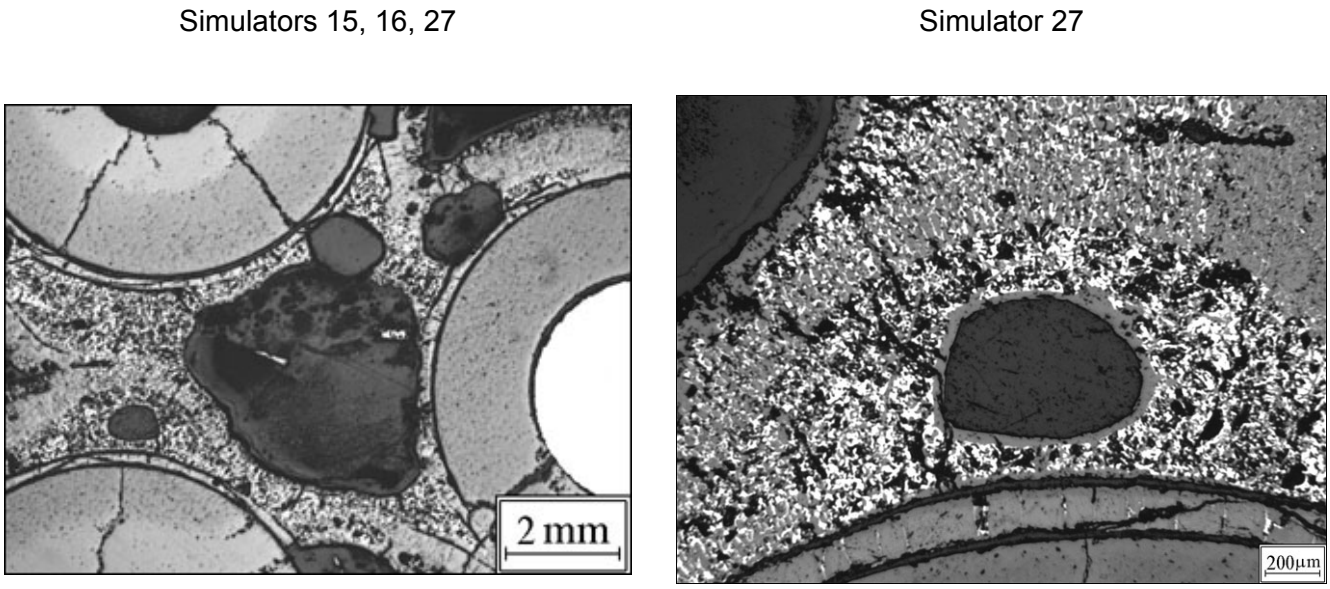

Fig. 11. Melt structure in section 954 mm.

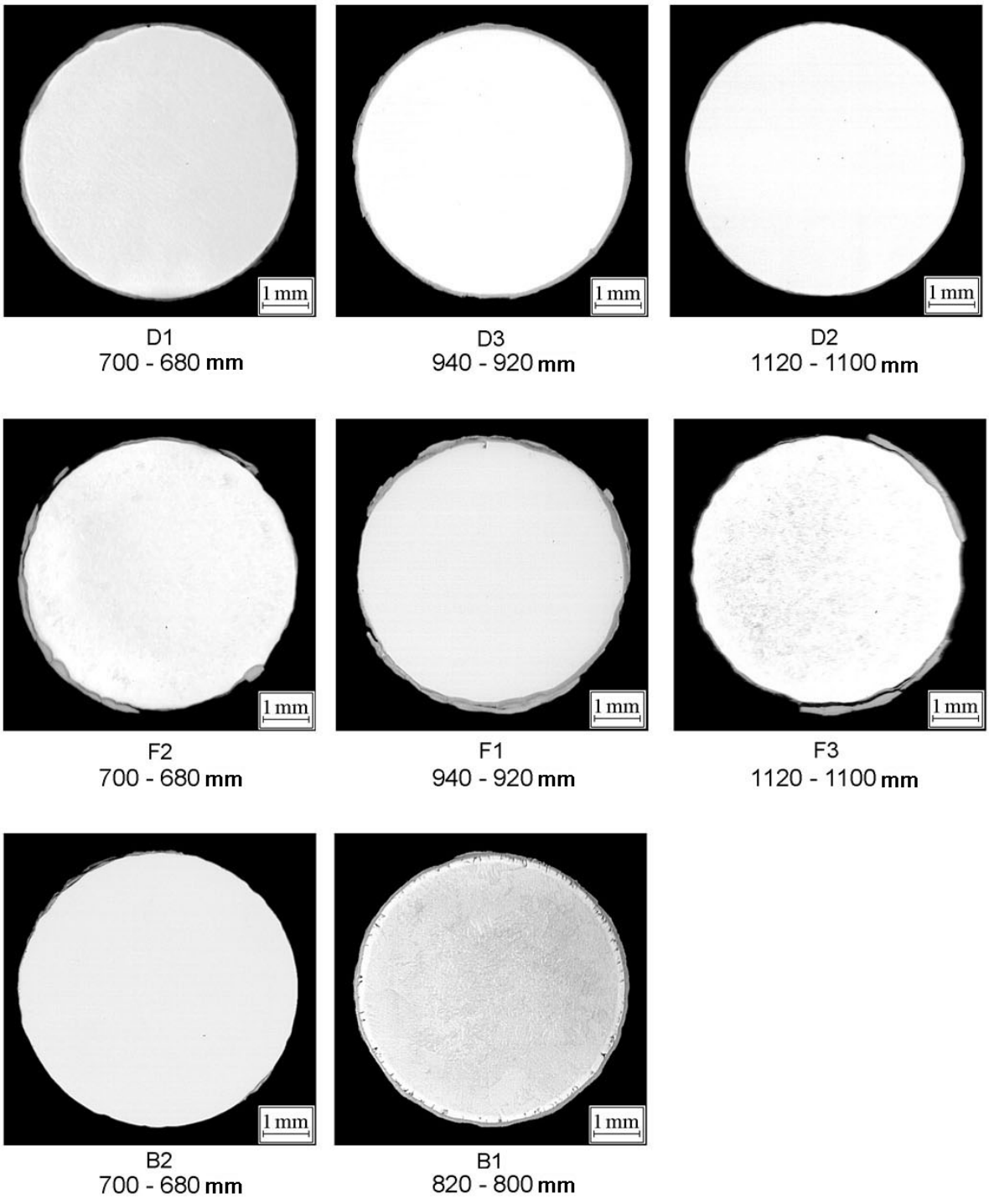

Fig. 12. Pictures of the examined rod sections.

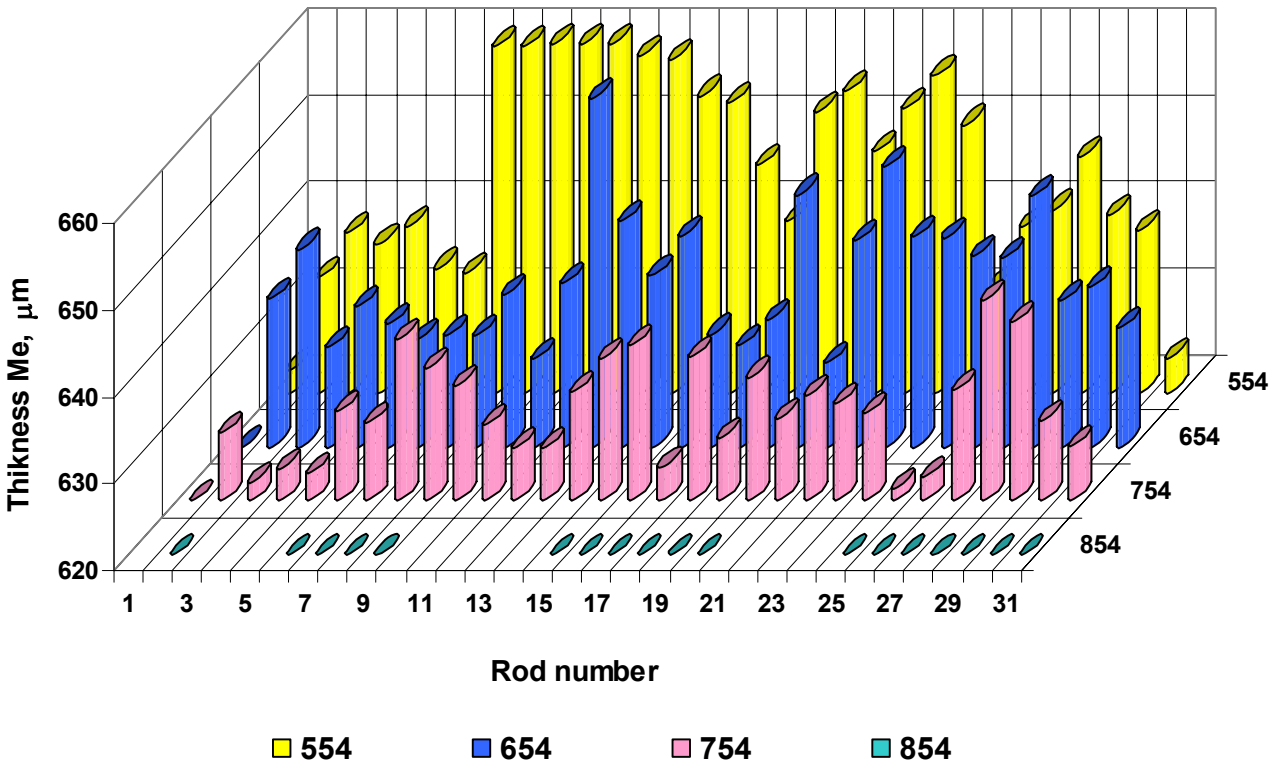

Fig. 13. Diagram of changes in the thickness of the metal part of the simulator claddings in the examined sections.

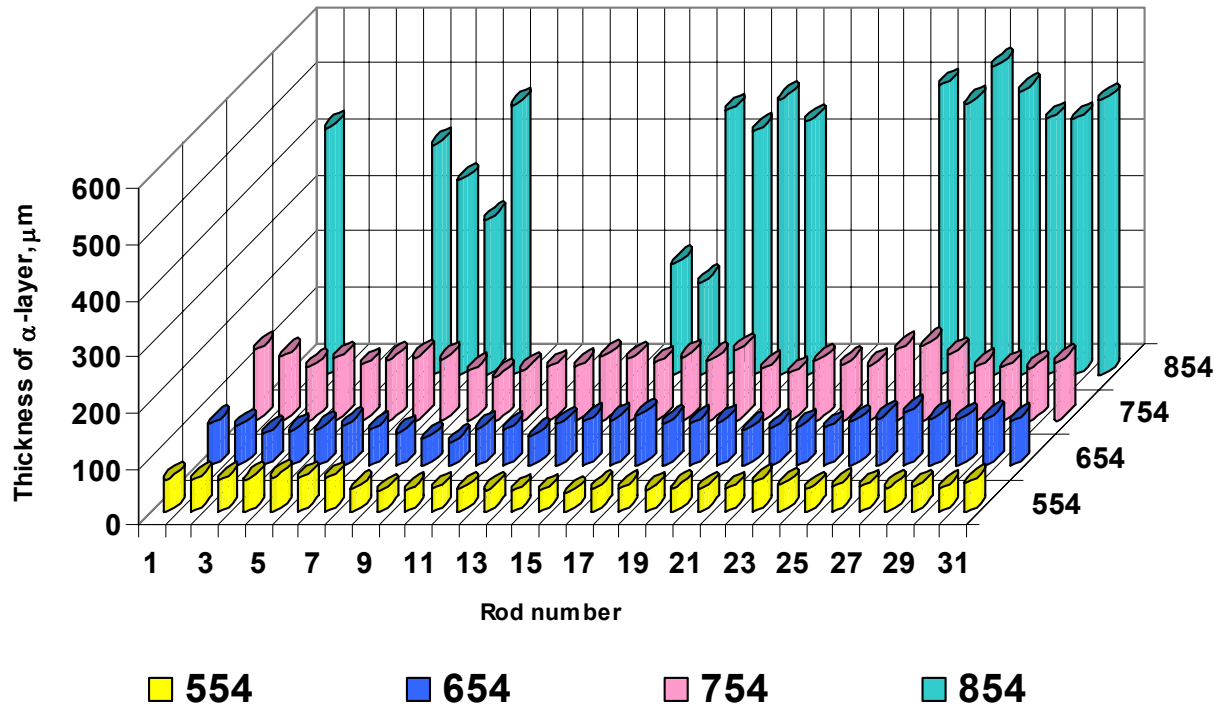

Fig. 14. Diagram of α–Zr(O) thickness change in the examined sections.